Available online at www.sciencedirect.com

SciVerse ScienceDirect

Advances in Space Research 50 (2012) 1629–1637

ADVANCES IN SPACE RESEARCH (a COSPAR publication)

www.elsevier.com/locate/asr

The South Pole-Aitken basin region, Moon: GIS-based geologic investigation using Kaguya elemental information

Kyeong Ja Kim [a,*], James M. Dohm [b], Jean-Pierre Williams [c], Javier Ruiz [d], Trent M. Hare [e], Nobuyuki Hasebe [f], Yuzuru Karouji [g], Shingo Kobayashi [h], Makoto Hareyama [g], Eido Shibamura [i], Masanori Kobayashi [j], Claude d'Uston [k], Olivier Gasnault [k], Olivier Forni [k], Sylvestre Maurice [k]

[a] *Geological Research Division, Korea Institute of Geosciences & Mineral Resources, Daejeon, South Korea*
[b] *Department of Hydrology and Water Resources, University of Arizona, Tucson, AZ 85721, USA*
[c] *Department of Earth and Space Sciences, University of California, Los Angeles, CA 90095, USA*
[d] *Departamento de Geodinámica, Facultad de Ciencias Geológicas, Universidad Complutense de Madrid, 28040 Madrid, Spain*
[e] *U.S. Geological Survey, Flagstaff, AZ 86001, USA*
[f] *Research Institute for Science and Engineering, Waseda University, Shinjuku, Tokyo 169-8555, Japan*
[g] *Japan Aerospace Exploration Agency, Sagamihara, Kanagawa 229-8510, Japan*
[h] *National Institute of Radiological Sciences, Inage, Chiba, Japan*
[i] *Saitama Prefectural University, Saitama 343-8540, Japan*
[j] *Chiba Institute of Technology, Narashino, Chiba 275-0016, Japan*
[k] *Universite de Toulouse; UPS-OMP; CNRS; IRAP; 9 Av. colonel Roche, F-31028 Toulouse cedex 4, BP 44346, France*

Available online 28 June 2012

Abstract

Using Geographic Information Systems (GIS), we performed comparative analysis among stratigraphic information and the Kaguya (SELENE) GRS data of the ~2500-km-diameter South Pole-Aitken (SPA) basin and its surroundings. Results indicate that the surface rock materials (including ancient crater materials, mare basalts, and possible SPA impact melt) are average to slightly elevated in K and Th with respect to the rest of the Moon. Also, this study demonstrates that K and Th have not significantly changed since the formation of SPA. The elemental signatures of the impact basin of Fe, Ti, Si, O through time include evidence for resurfacing by ejecta materials and late-stage volcanism. The oldest surfaces of SPA are found to be oxygen-depleted during the heavy bombardment period relative to later stages of geologic development, followed by both an increase in silicon and oxygen, possibly due to ejecta sourced from outside of SPA, and subsequent modification due to mare basaltic volcanism, which increased iron and titanium within SPA. The influence of the distinct geologic history of SPA and surroundings on the mineralogic and elemental abundances is evident as shown in our investigation.

Keywords: Kaguya (SELENE); Gamma-Ray Spectrometer; South Pole-Aitken basin; Elemental maps; Impact

* Corresponding author. Address: Geological Research Division, Korean Institute of Geoscience and Mineral Resources, 124 Gwahang-no, Yuseong-gu, Daejeon 305-350, Republic of Korea. Tel.: +82 42 868 3669; fax: +82 42 868 3413.

E-mail addresses: kjkim@kigam.re.kr (K.J. Kim), jmd@hwr.arizona.edu (J.M. Dohm), jpierre@mars.ucla.edu (J.-P. Williams), jaruiz@geo.ucm.es (J. Ruiz), thare@usgs.gov (T.M. Hare), nhasebe@waseda.jp (N. Hasebe), karouji@planeta.sci.isas.jaxa.jp (Y. Karouji), shingo@nirs.go.jp (S. Kobayashi), hareyama.makoto@jaxa.jp (M. Hareyama), shibamura-eido@spu.ac.jp (E. Shibamura), kobayashi.masanori@it-chiba.ac.jp (M. Kobayashi), lionel.duston@cesr.fr (C. d'Uston), Olivier.Gasnault@cesr.fr (O. Gasnault), Olivier.Forni@cesr.fr (O. Forni), sylvestre.maurice@cesr.fr (S. Maurice).

0273-1177/$36.00
http://dx.doi.org/10.1016/j.asr.2012.06.019

1. Introduction

Large impact events have significantly influenced the geologic history of the Moon. The South Pole-Aiken (SPA) basin is one such event that resulted in a ~2500-km-diameter impact basin during the pre-Nectarian period (Figs. 1 and 2). The basin is the largest unambiguously recognized impact structure in the Solar System, centered at 56°S, 180° on the farside of the Moon (Wilhelms, 1987; Spudis et al., 1994). The SPA basin region is one of two lunar regions with distinctive elemental abundances (e.g., Fe) when compared to other parts of the Moon (e.g., Lawrence et al., 1998, 2000; Elphic et al., 2000; Jolliff et al., 2000; Prettyman et al., 2006). In addition, Lunar-Prospector-based high thermal neutron intensities generally delineate the basin (Feldman et al., 1998). The other region, which is much more distinct in elemental signature (e.g., elevated in Th, K, Mg, U, and Ti in addition to Fe), is the pre-Nectarian 3200-km-diameter Procellarum basin (referred to hereafter as PKT) (Fig. 1), which is the site of one of the largest hypothesized impact basins in the solar system (Cadogan, 1974). The SPA basin floor is uniquely mafic (Jolliff et al., 2000). FeO and TiO_2 concentrations in the SPA basin region indicate the presence of possible upper mantle materials (Lucey et al., 1998) or noritic (lower crust) material (Pieters et al., 1997). Noritic material is also seen in the central peaks in SPA impact-melt (Nakamura et al., 2009). Whereas PKT has been highly resurfaced by post-Nectarian geologic activity, which includes impact cratering events (e.g., Imbrium and Serenitatis) and voluminous mare-forming volcanism (Wilhelms, 1987), the pre-Nectarian surfaces have been much less obscured in the South Pole-Aiken basin region, which includes possible impact melt exposed on the basin floor (Kreslavsky et al., 2001; Pieters et al., 2001, 2003), in addition to other material types emplaced following the impact event (Spudis, 2009). Localized mare volcanic materials permit individual stages of emplacement to be isolated and investigated for variations in age, morphology (Whitford-Stark, 1979; Hawke et al., 1990), and composition (Spudis et al., 1984; Gaddis et al., 1995).

In this work, we performed a comparative analysis among the stratigraphy, as defined using published USGS geologic maps (Wilhelms and McCauley, 1971; Wilhelms and El-Baz, 1977; Scott et al., 1977; Stuart-Alexander, 1978; Lucchitta, 1978; Wilhelms et al., 1979), and the Kaguya (SELENE) Gamma Ray Spectrometer (hereafter referred to hereafter as KGRS) elemental information of the SPA basin region using Geographic Information Systems (GIS). From this, we attempt to delineate the pre-Nectarian and Nectarian materials from the younger mare-forming volcanic materials to investigate whether they are distinct in elemental signature from one another and from materials outside of the basin region.

2. Methodology

Our method to compare the geologic evolution of the SPA basin region with elemental data requires that we determine the spatial and temporal extent of the rock materials (mapped units) and the total area of the SPA basin region (Fig. 1). To determine the temporal extent of the SPA basin region, our approach requires the definition of major stages of geologic activity for the region. Based on the geologic investigation of Wilhelms (1987), which includes absolute-age information determined from Apollo rock samples, we choose Pre-Nectarian and Nectarian activity, which includes surfaces resulting from the SPA event (stage 1), the Imbrium and Orientale impact events (stage 2), and mare volcanism (stage 3) that occurred subsequent to the Imbrium and Orientale impact events as the major stages of geologic activity of the Moon (Fig. 2). The

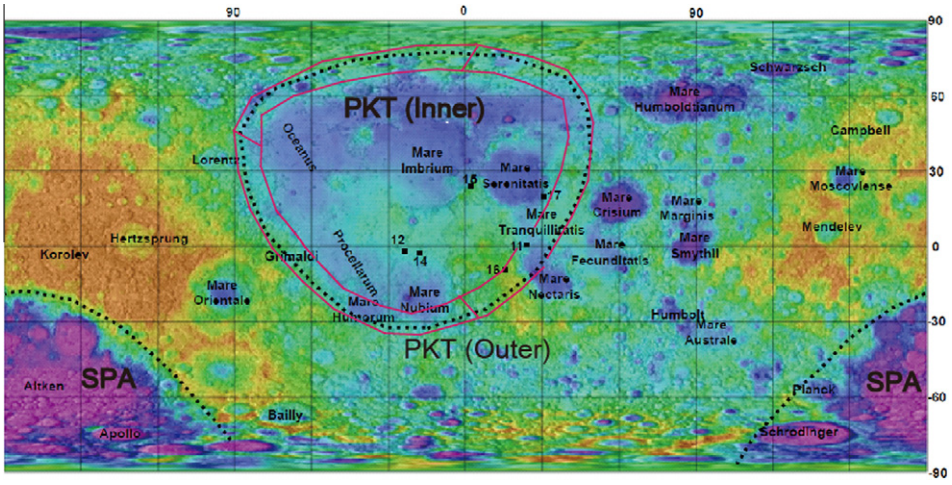

Fig. 1. Combined ILCN2005_lpo topography and shaded relief warp mosaic showing impact craters, which includes the extent of the SPA basin and hypothesized Procellarum basin, as defined by Wilhelms (1987). Note that the outlined South Pole-Aitken basin (SPA) is the primary focus of our GIS-based investigation. Procellarum-Imbrium basin region (PKT Inner), Procellarum-Imbrium basin margin region (between the red lines; PKT Outer), and South Pole-Aitken basin are the primary regions for comparative analysis using GIS.

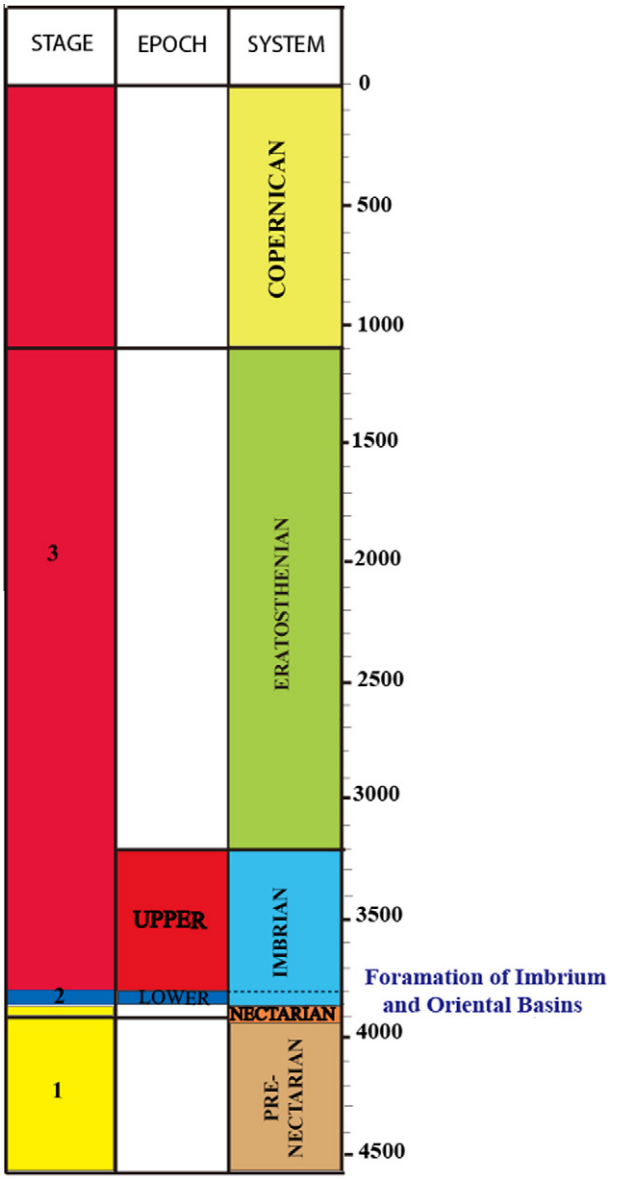

Fig. 2. Lunar geologic timescale. Also shown is stage information correlated with Epoch and System information based from Wilhelms (1987). See Section 2 for stage information.

stage 1 type locality is Apollo 17 with returned rock samples estimated to be 4.5 Ga, the stage 2 type locality is Apollo 14 with returned rock samples estimated to be of 3.9 Ga, and the stage 3 type locality is Apollo 12 with returned rock samples estimated to be 3.5 Ga.

For simplicity, we separate the geologic materials into 3 stages rather than 6 stages as proposed in the "Apollo Model 2000" (Schmitt, 1999). The rationale is that we want to investigate whether the Pre-Nectarian and Nectarian impact cratering events and related regolith mixing are distinct from the Imbriam and Orientale impact events and subsequent mare volcanism. Based on this, each map unit of the published USGS geologic maps, L-0703 (Wilhelms and McCauley, 1971), L-0948 (Wilhelms and El-Baz, 1977), L-1034 (Scott et al., 1977), L-1047 (Stuart-Alexander, 1978), L-1062 (Lucchitta, 1978), and L-1162 (Wilhelms et al., 1979) is assigned a stage for GIS-based compilation (Figs. 3 and 4; Table 1). For example, the pre-Nectarian polygons were assigned stage 1, the Lower Imbrian polygons related to the Orientale and Imbrium impact events stage 2, and the Upper Imbriam units related to Mare-forming volcanism stage 3 (Figs. 2 and 3). Other Upper Imbriam, Eratosthenian, and Copernican map units were also assigned stage 3, as they were emplaced following the Imbrium and Orientale impact events.

Using Geographic Information Systems (GIS), the areal extent of polygons of a specific stage can then be readily compiled for comparison with the elemental information. For example, we calculated (Table 2): (1) the total area of the SPA basin region (Fig. 1), (2) the total area of stage 1, stage 2, and stage 3 materials within the SPA basin region, outside of the SPA basin region, and for all of the Moon, and (3) the average elemental abundance of each stage of materials (e.g., mare lavas vs. older highland cratered materials) within the SPA basin region, and outside the SPA region, as well as for all of the Moon, using elemental information acquired by the Kaguya Gamma Ray Spectrometer (KGRS), including counts per minute (cpm) of Th, K, Fe, Si, Ti, and O (Fig. 5). In (3), for example, the relative abundance of K for post-Orientale impact material (e.g., mare lavas) can be readily determined from the KGRS counts using GIS (likened to a "cookie cut out" of the stage 3 materials and using the cut out to determine its average K counts per minute (cpm)). This information then can be readily compared with the other regions (e.g., the average K counts of the cratered highland materials within the SPA basin vs. the cratered highland materials outside the basin, etc.). A similar GIS-based approach has been used for Mars to assess the geologic evolution of the Thaumasia region (Dohm et al., 1998, 2001, 2007; Tanaka et al., 1998), to compare two giant shield complexes, Syria Planum and Alba Patera (Anderson et al., 2004), and to investigate the possible existence of large bodies of water through Mars Odyssey Gamma Ray Spectrometer data (Dohm et al., 2009).

Here, we perform a comparative analysis among stratigraphy and KGRS natural radioactive elemental (K and Th) (Figs. 6–8) and major elemental (Fe, Ti, Si, and O) data (Figs. 9–11) using GIS (calibrated maps of Mg, Ca, and Al are not yet available). We have chosen to use KGRS data for our comparative analysis rather than LPGRS because the KGRS instrument provides a more detailed gamma-ray spectrum (Fig. 5). The Kaguya mission is the first to employ a High Purity Germanium (HPGe) detector to observe lunar Gamma Rays (Hasebe et al., 2008, 2009; Karouji et al., 2008; Kobayashi et al., 2005, 2010; Yamashita et al., 2010) (Fig. 5). Thus, the KGRS instrument can provide much more detailed gamma-ray spectra (higher energy resolution), and as such, KGRS can detect many more gamma ray peaks than the Lunar Prospector Gamma-Ray Spectrometer (LPGRS). This results in much improved elemental maps (for more information, see

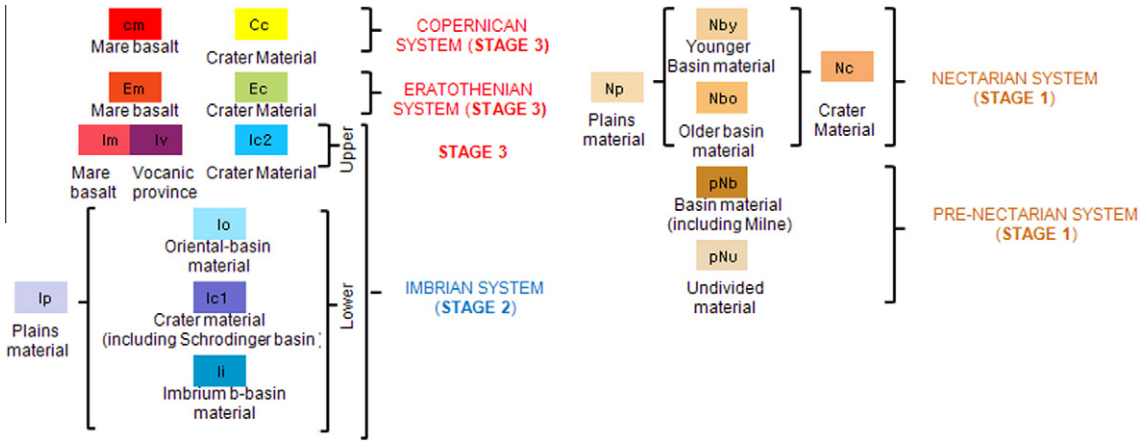

Fig. 3. Modified from Wilhelms (1987), correlation chart showing stratigraphic positions of the units. Also shown are the major stages of geologic activity for the Moon, which form the basis for performing comparative analysis among the stratigraphy and KGRS elemental information. The stages include: (stage 1) the pre-Nectarian impact events, hypothesized Procellarum and SPA, as well as the heavy bombardment during the Nectarian to form large impact basins such as Crisium, Humboldtianum, Serenitatis, Nectaris, and Humorum, all of which are on the nearside, and Mendeleev, Moscoviense, Korolev, and Hertzsprung on the far side; (stage 2) Lower Imbriam impact events, Orientale and Imbrium, and (stage 3) Upper Imbriam Mare-forming volcanism (post Late Heavy Bombardment (LHB)).

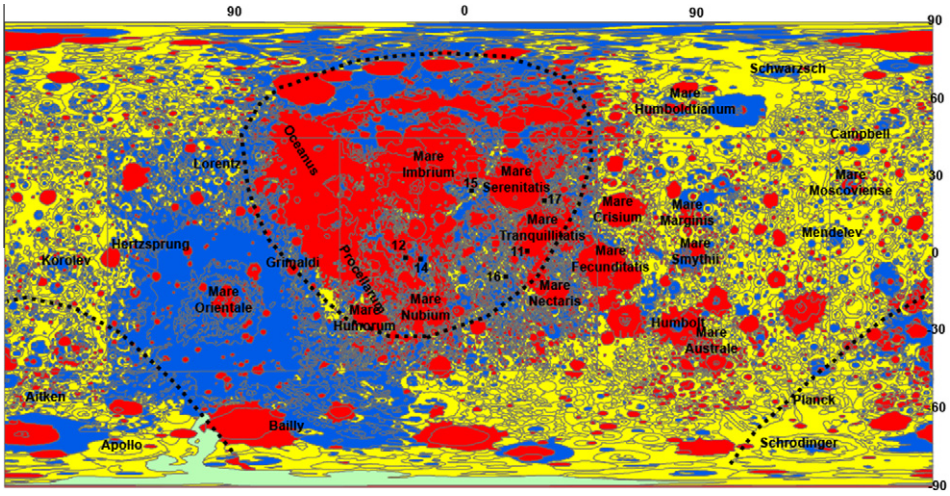

Fig. 4. Stage 1 (yellow), stage 2 (blue), and stage 3 (red) assignments of the map units of published USGS geologic maps, L-0703 (Wilhelms and McCauley, 1971), L-0948 (Wilhelms and El-Baz, 1977), L-1034 (Scott et al., 1977), L-1047 (Stuart-Alexander, 1978), L-1062 (Lucchitta, 1978), and L-1162 (Wilhelms et al., 1979). Note that the uncolored areas were not defined on the digital maps. Also delineated are the South Pole Aitken (SPA) and putative Procellarum impact basins. (For interpretation of the references to colour in this figure legend, the reader is referred to the web version of this article.)

Table 1
Stage assignment of map units of published USGS geologic maps, L-0703 (Wilhelms and McCauley, 1971), L-0948 (Wilhelms and El-Baz, 1977), L-1034 Scott et al., 1977), L-1047 (Stuart-Alexander, 1978), L-1062 (Lucchitta, 1978), and L-1162 (Wilhelms et al., 1979). Note that Stage 1 denotes Pre-Nectarian and Nectarian (period of heavy bombardment, Stage 2 represents the Imbrium and Orientale impact events and associated materials, and Stage 3 activity that occurred following the Imbrium and Orientale impact events such as mare volcanism.

Stage	Map units
3	CC, Cc1, Cc2, Ccc, CEch, CEci, CEd, Cehf, Cf, Cld, Cp, Csc, Ec, Ecc, Eld, Elm, Elph, Em, Emd, Emp, Esc, Ic, Ic2, Icc, Icc2, Ics, Id, Ifc, Im, Im1, Im2, Imd, Ip2, Irc, Isc, It
2	Ia, Ial, Iap, Ic1, Icc1, Ich, Ici, Ico, If, Ig, Ih, Ihe, Ihf, Ihp, Iic, Inbl, Infp, Inp, Int, Ioc, Iohi, Iohn, Ioho, Iohs, Ioht, Iom, Iork, Iorm, Ip, Ip1, Iplt, IpNbm, IpNcl, IpNg, IpNI, IpNt
1	Nb, Nbc, Nbh, Nbl, Nbm, Nc, Ncc, Nhb, Nhsc, Nj, Np, NpNbm, NpNbr, NpNhf, NpNt, Npnt, Nsc, Nt, Ntp, pbr, plc, plc1, plc2, plc3, plch, plci, plj, pl1, plp, plr, pNb, pNbm, pNbr, pNc, pNcc, pNt

Reedy et al. (2009)). In a 100 km lunar polar orbit, the GRS onboard the Kaguya spacecraft has acquired elemental information of the surface of the Moon, including gamma rays from Al, Mg, Si, Ca, Ti, Fe, Th, and U.

Table 2
GIS-based areas of seven regions defined for this study. The summed areas associated as each stage in the seven regions are demonstrated.

Region	Total area (million km^2)	Total area for each stage (million Km^2)		
		1	2	3
PKT (Inner)	4.4	0.2	0.8	3.4
PKT (Outer)	2.5	0.2	1.1	1.2
Whole PKT (Inner & Outer)	6.9	0.5	1.9	4.5
Outside PKT (Total Moon minus Inner & Outer)	30.9	16.6	8.6	5.0
SPA	3.8	1.9	1.0	0.6
Outside SPA (Total Moon minus SPA)	34.0	15.1	9.5	9.0
Total Moon	37.8	17.0	10.5	9.6

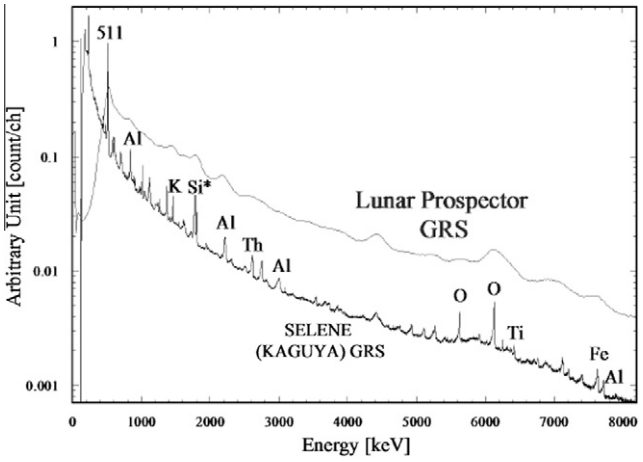

Fig. 5. Comparison of energy spectra obtained by SELENE (KAGUYA) GRS and Lunar Prospector GRS (Hasebe et al., 2009).

Compared to the 150 km spatial resolution of the LPGRS, the KGRS has a spatial resolution of 135 km.

3. Results and discussion

From an elemental perspective, when compared to the rest of the Moon (Fig. 1), the SPA basin region is one of two elementally distinct regions (the other is PKT), which includes enrichment in Fe, FeO, and TiO_2 (e.g., Lucey et al., 1995), and Mg (Hiesinger and Head, 2004; Spudis, 2009). Our GIS-based results indicate that the materials within the basin region on average exhibit similar K and Th abundances when compared to those outside of the basin region (Fig. 9), though there are visibly local highs and lows in the counts. Very little change in K and Th counts through time indicate that SPA materials have remained homogeneous relative to K and Th since the basin-forming impact.

We gain additional perspective of the surface evolution of SPA and surrounding regions through the major elements of Fe, Ti, Si, and O, which have the lowest counts per minute (cpm) in stage 1. The subsequent increase in these elemental abundances is interpreted to result from post-SPA impact cratering and mare basaltic volcanism (Figs. 10 and 11).

We also find a similar modest increase in counts per minute (cpm) for both Ti and Fe between stage 1 and stage 2 for all regions (Fig. 10). In the case of the SPA region, Si counts in stage 1 are lowest, possibly indicating relatively more mafic surfaces than stage 3, even when mare basaltic volcanism is observed to have occurred, with the highest amount of Si found in stage 2 (Fig. 11). O is clearly shown to be depleted during stage 1 of SPA with respect to the

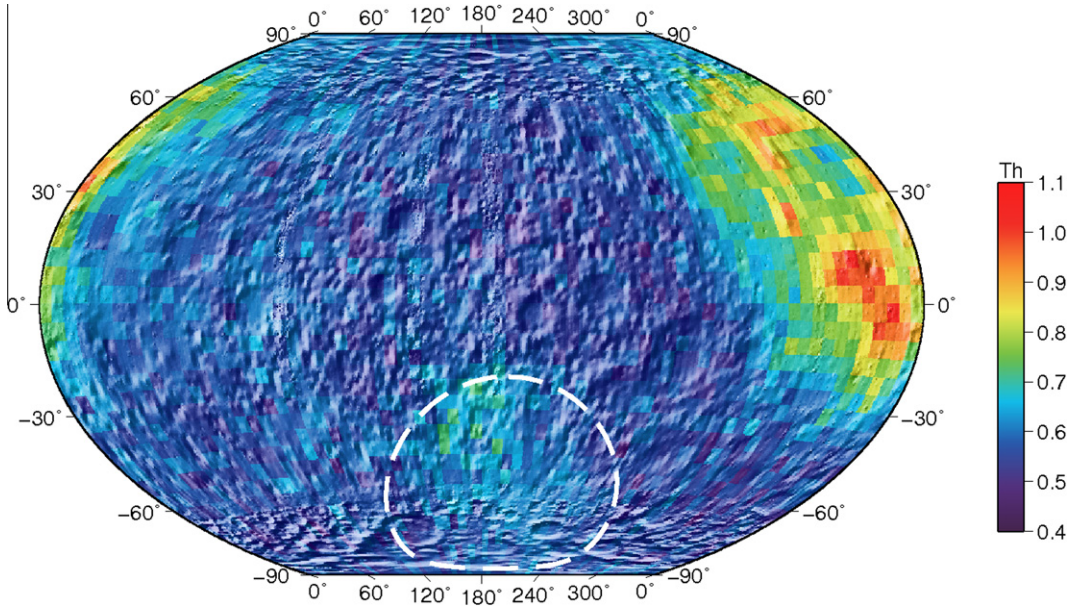

Fig. 6. Modified from Kobayashi et al. 2010. Color-coded map of the Th with original count rate (counts/second) at channel 597 (911 keV) representative of the Thorium line. Note that the SPA basin (dashed line) is relatively indistinct in Th.

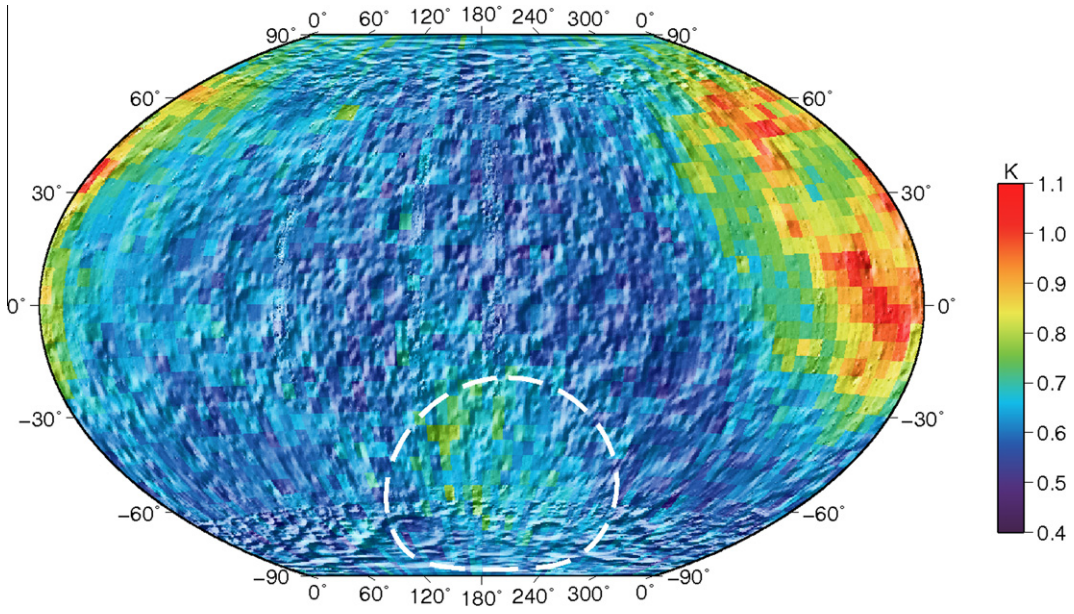

Fig. 7. Modified from Kobayashi et al. (2010). The global map of K gamma-ray counting rate (in counts per second) as measured by KGRS. Note that the SPA basin (dashed line) is relatively indistinct in K.

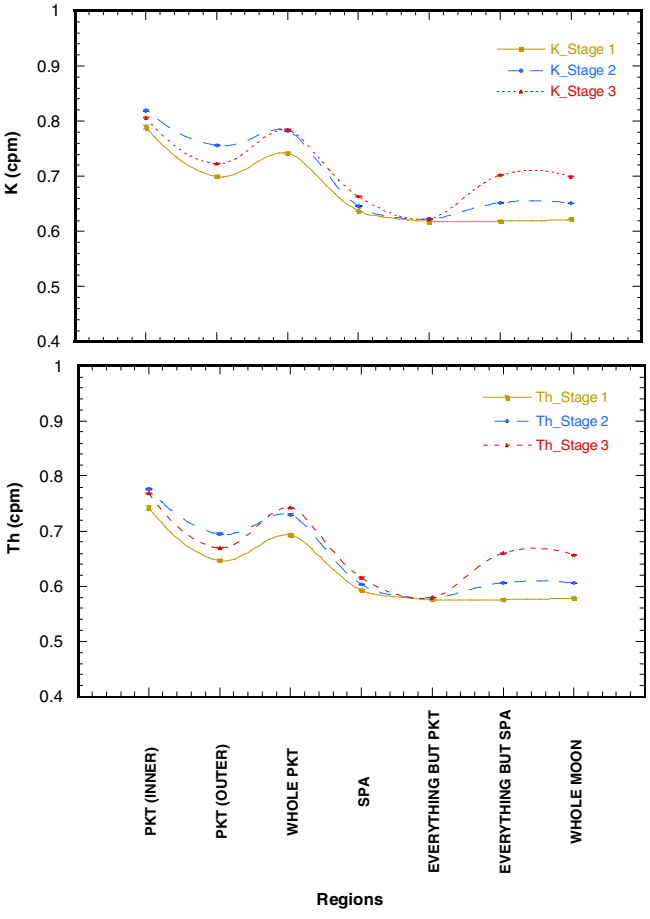

Fig. 8. The two plots show the average count per minute (cpm) of K and Th for each of the regions of interest, respectively. Error bars show the standard deviation of the mean for each region. Note that total SPA basin region is relatively indistinct from the region outside of the SPA basin region (everything but SPA) and the whole Moon.

later stages of activity and relative to the rest of the lunar surface.

The O:Si ratio (cpm/cpm) in Fig. 12 tells us something about broad evolutionary trends in the predominant silicate structure of the minerals present. The O:Si ratio will increase from quartz/feldspar to olivine. The O:Si ratio is highest in stage 1 and lowest in stage 2 indicating a shift toward more felsic surfaces in stage 2 with stage 1 being the most mafic.

4. Summary

Through a general inspection of the KGRS Th and K counts, the Moon appears fairly homogeneous with the exception of two anomalous regions PKT and SPA. While the counts for K and Th in SPA are elevated relative to the rest of the Moon, excluding PKT, they do not vary in a significant way between stages implying the crust was not enriched, at least at the resolution of our maps, significantly with the incompatible elements with time. Similarly, we find only minor variations in both Fe and Ti in the SPA region since the formation of the basin, although the observed increase in counts in stage 3 is consistent with volcanic resurfacing in the basin. The decrease in the O:Si ratio from stage 1 to stage 2 implies a generally more felsic surface in stage 2 relative to the older stage 1 materials. This could result from resurfacing by ejecta material originating from regions exterior to the basin that source from shallower depth of the lunar crust. The ratio increases slightly in stage 3 consistent with the occurrence of mafic volcanism. This is also seen as higher Si counts in stage 2 relative to the other stages. The anomalously low oxygen counts in stage 1 of SPA basin indicate ultra-mafic materials may have been exposed after the SPA impact event.

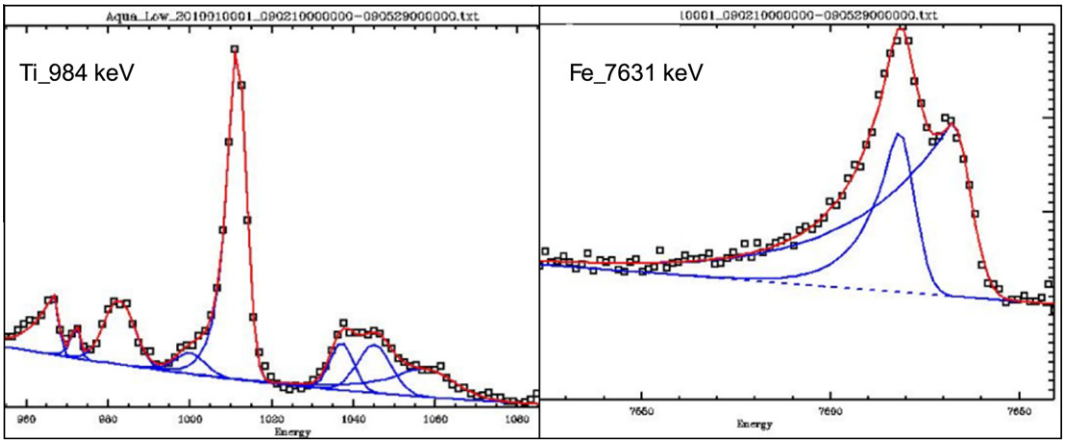

Fig. 9. The gamma-ray analysis program Aquarius was used, which is developed by CESR (Centre d'Etude Spatiale des Rayonnements).

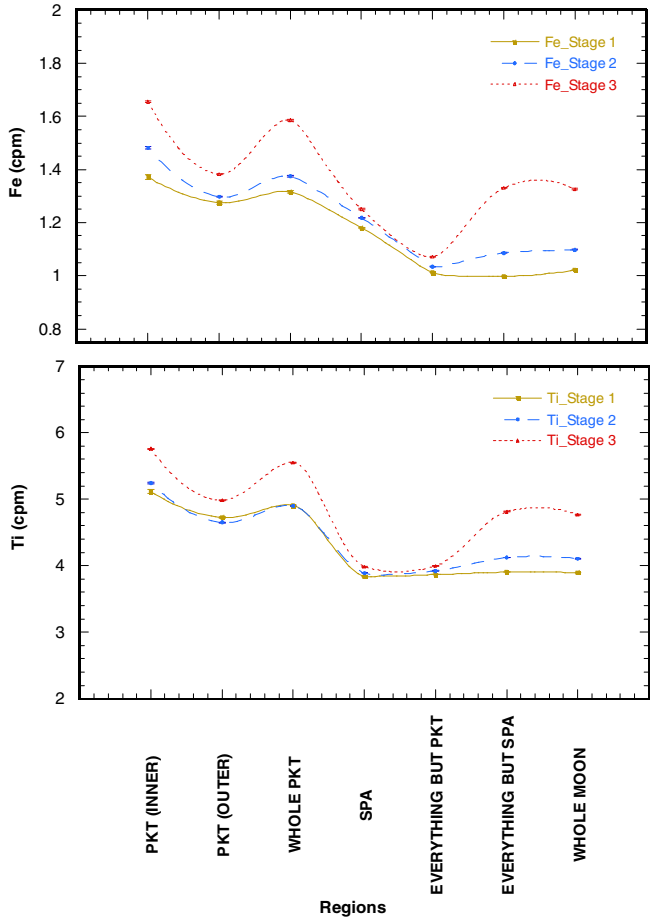

Fig. 10. The two plots show the average count per minute (cpm) of Fe and Ti for each of the regions of interest, respectively. Error bars show the standard deviation of the mean for each region. This plots show an increase in both Fe and Ti concentrations in SPA during stages 2 and 3 interpreted to mark resurfacing by both impact cratering and volcanism during stages 2 and 3, respectively.

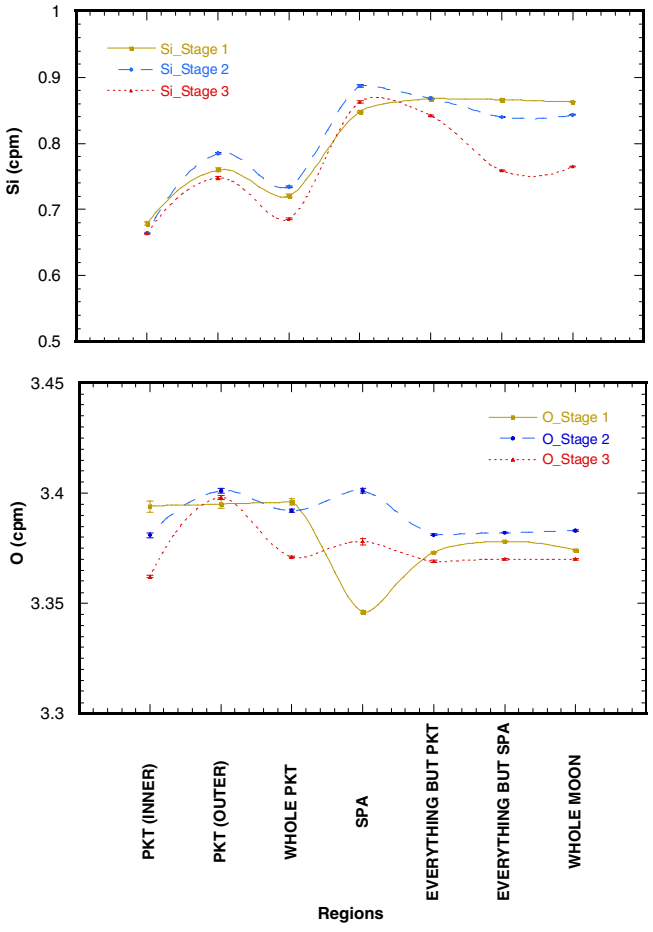

Fig. 11. The two plots show the average count per minute (cpm) of Si and O for each of the regions of interest, respectively. Error bars show the standard deviation of the mean for each region. The Si plot shows that Si has been significantly increased in Stage 2 (heavy bombardment period) and stage 1 Si concentration was lower than that of stages 2 and 3. We interpret this to mark resurfacing of SPA rock materials by both impact cratering and mare basaltic volcanism. This later resurfacing is also apparent in the O plot. Stage 1 rock materials are clearly depleted in O with more elevated concentrations of O during stages 2 and 3, also interpreted to mark partial resurfacing by impact cratering especially during stage 2 and less resurfacing by basaltic mare volcanism during stage 3 and less resurfaced during Stage 3 mare basaltic volcanism.

We interpret the results of our investigation as marking an ancient period (mostly pre-Nectarian) of impact crater mixing during the period of heavy bombardment (a large percentage of the rock surfaces reflect pre-Nectarian SPA

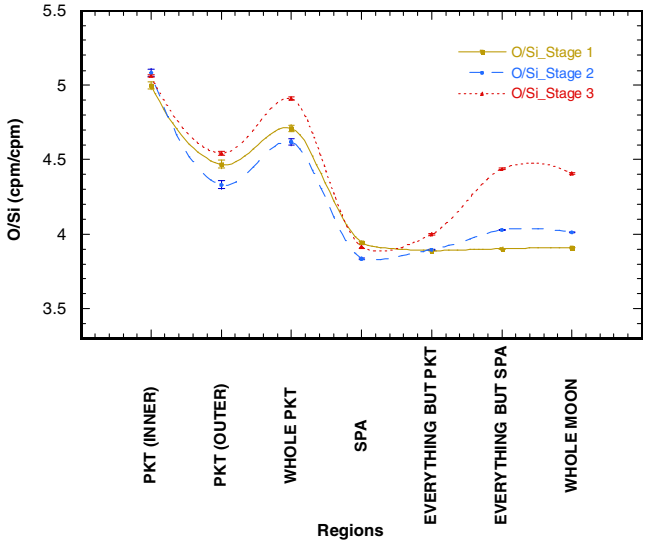

Fig. 12. O/Si ratio (cpm/cpm) for the lunar regions. Error bars show the standard deviation of the mean for each region. The low O/Si of all regions except SPA during stage 3 shows that the Moon has been influenced by volcanic activity during a later stage. In addition, the low O/Si may indicate that the mare and highland materials were partly covered by low-Si materials.

and subsequent impact crater events of regional extent outside of SPA basin region such as Orientale). Unlike PKT, which was highly modified by impact events such as Imbrium and mare volcanism, the ancient record of the SPA region was not significantly subdued. Compared with the magma generation in PKT of the nearside, the unproductive generation in the farside mantle, as pointed out by Taylor (2009), could be explained by a lack of relatively large impacts such as Imbrium to reactivate faults and provide a source of heat to possibly remelt part of the lunar interior and/or tap into magma sources from the lower crustal/mantle boundary. Thus, this study demonstrates that the elemental signatures of major elements of SPA, coupled with GIS investigations to provide temporal information, provide insight into potential chemical evolutionary trends in the basin's geology.

Acknowledgements

This work was supported by a research project, '12-3612' at the Korea Institute of Geoscience and Mineral Resources funded by the Ministry of Knowledge Economy of Korea and 10-6303 at funded by Ministry of Education, Science, and Technology of Korea. Dr. Javier Ruiz was supported by a contract Ramón y Cajal co-financed from the Ministerio de Ciencia e Innovación of Spain and the Fondo Social Europeo (ESF).

References

Anderson, R.C., Dohm, J.M., Haldemann, A.F.C., et al. Tectonic histories between Alba Patera and Syria Planum. Mars. Icarus 171, 31–38, 1974.

Cadogan, P.H. Oldest and largest lunar basin? Nature 250 (5464), 315–316, 1974.

Dohm, J. M., Anderson, R. C., Tanaka, K. L. Digital Structural Mapping of Mars. Astron. Geophys. 39, 3.20–3.22, 1998.

Dohm, J. M., Tanaka, K. L., Hare, T. M. Geologic map of the Thaumasia region of Mars. USGS Misc. Inv. Ser. Map I-2650, scale 1:5000,000, 2001.

Dohm, J. M., Maruyama, S., Baker, V. R., et al. Traits and evolution of the Tharsis superplume, Mars. In Superplumes: beyond plate tectonics: Yuen, D. A., Maruyama, S., Karato, S.-I., Windley, B. F. (eds.). Springer, 523–537, 2007.

Dohm, J.M., Baker, V.R., Boynton, W.V., et al. GRS evidence and the possibility of paleooceans on Mars. Planet. Space Sci. 57, 664–684, 2009.

Elphic, R.C., Lawrence, D.J., Feldman, W.C., et al. Lunar rare earth elements distribution and ramifications for FeO and TiO2: Lunar Prospector neutron spectrometer observations. J. Geophys. Res. 105, 20333–20345, 2000.

Feldman, W.C., Barraclough, B.L., Maurice, S., et al. Major compositional units of the Moon: Lunar Prospector thermal and fast neutrons. Science 281, 1489–1493, ldman et al., 2.

Gaddis, L.R., McEwen, A.S., Becker, T.L. Compositional variations on the Moon: recalibration of Galileo solid-state imaging data for the Orientale region and farside. J. Geophys. Res. 100, 26345–26355, 1995.

Hasebe, N., Shibamura, E., Miyachi, T., et al. Gamma-Ray Spectrometer (GRS) for Lunar Polar Orbiter SELENE. Earth Planets Space 60, 299–312, 2008.

Hasebe, N., Shibamura, E., Miyachi, T., et al. First Results of High Performance Ge Gamma-Ray Spectrometer Onboard Lunar Orbiter SELENE (KAGUYA). J. Phys. Soc. Jpn. 78, 18–25 (Supplement A), 2009.

Hawke, B.R., Lucey, P.G., Bell, J.F., et al. Ancient mare volcanism, LPI-LAPST Workshop on Mare Volcanism and Basalt Petrogenesis: Astounding Fundamental Concepts (AFC) Developed Over the Last Fifteen Years, 5–6, 1990.

Hiesinger, H., Head, J.W. Lunar South Pole-Aitken impact basin: topography and mineralogy. LPSC XXXV, abstr 1164, 2004.

Jolliff, B.L., Gillis, J.J., Haskin, L.A., et al. Major lunar crustal terranes: surface expressions and crust-mantle origins. J. Geophys. Res. 105, 4197–4216, 2000.

Karouji, Y., Hasebe, N., Okudaira, O., et al. Distributions of K and Th on the Moon: the initial results from observations by SELENE GRS. Adv. Geosci. 18, 43–55, 2008.

Kobayashi, M.-N., et al., Global mapping of elemental abundance on lunar surface by SELENE Gamma-Ray Spectrometer. LPSC XXXVI, abstr 2092, 2005.

Kobayashi, S., Hasebe, N., Shibamura, E., et al. Determining the absolute abundances of natural radioactive elements on the lunar surface by Kaguya Gamma-Ray Spectrometer. Space Sci. Rev. 154, 193–218, http://dx.doi.org/10.1007/s11214-010-9650-2, 2010.

Kreslavsky, M.A., Shkuratov, Y.G., Velikodsky, I., et al. Photometric properties of the lunar surface derived from Clementine observations. J. Geophys. Res. 105 (E8), 20281–20296, 2001.

Lawrence, D.J., Feldman, W.C., Barraclough, B.L., et al. Global elemental maps of the Moon: the Lunar Prospector Gamma-Ray Spectrometer. Science 281, 1484–1489, 1998.

Lawrence, D.J., Feldman, W.C., Barraclough, B.L., et al. Thorium abundances on the lunar surface. J. Geophys. Res. 105, 20307–20331, 2000.

Lucchitta, Geologic map of the north side of the Moon. USGS Map I-1062, scale 1:5000,000, 1978.

Lucey, P.G., Taylor, G.J., Malaret, E. Abundance and distribution of iron on the Moon. Science 26, 1150–1153, 1995.

Lucey, P.G., Taylor, G.J., Hawke, B.R., et al. FeO and TiO_2 concentrations in the South Pole-Aitken basin: implications for mantle composition and basin formation. J. Geophys. Res. 103, 3701–3708, 1998.

Nakamura, R., Matsunaga, T., Ogawa, Y., et al. Ultramafic impact melt sheet beneath the South Pole–Aitken basin on the Moon. Geophys. Res. Lett. 36, L22202, http://dx.doi.org/10.1029/2009GL040765, 2009.

Pieters, C.M., Tompkins, S., Head, J.W., et al. Mineralogy of the Mafic Anomaly in the South Pole-Aitken Basin: implications for excavation of the Lunar Mantle. Geophys. Res. Lett. 24, 1903–1906, 1997.

Pieters, C.M., Head, J.M., Gaddis, L., et al. Rock types of South Pole-Aitken basin and extent of basaltic volcanism. J. Geophys. Res. 106, 28001–28022, 2001.

Pieters, C.M., Duke, M., Head III, J.W., et al. Science options for sampling South Pole-Aitken basin. LPSC XXXIV, abstr 1366, 2003.

Prettyman, T. H., Hagerty, J. J., Elphic, R. C., et al. Elemental composition of the lunar surface. Analysis of gamma ray spectroscopy data from Lunar Prospector, J. Geophs. Res. 111, E12007, 1–41, 2006.

Reedy, R.C., Hasebe, N., Yamashita, N., et al. Gamma rays in spectra measured by the KAGUYA gamma-ray spectrometer. LPSC XXXX, abstr 1788, 2009.

Schmitt, H.H. Origin and Evolution of the Moon: Apollo 2000 Model, New Views of the Moon II, Flagstaff AZ, 22-44 Sept. 1999, abstr 1961, UWFDM-113, 1999.

Scott, D.H., McCauley, J.F., West, M.N. Geologic map of the west side of the Moon. USGS Map I-1034, scale 1:5000,000, 1977.

Spudis, P. Back to the Moon. Nature Geosci. 2, 234–236, 2009.

Spudis, P.D., Hawke, B.R., Lucey, P. Composition of Orientale basin deposits and implications for the lunar basin-froming process. J. Geophys. Res. 89, C197–C210, 1984.

Spudis, P.D., Reisse, R.A., Gillis, J.J. Ancient multiring basins on the Moon revealed by Clementine laser altimetry. Science 266, 1848–1851, 1994.

Stuart-Alexander, D.E. Geologic map of the central far side of the Moon. USGS Map I-1047, scale 1:5000,000, 1978.

Tanaka, K.L., Dohm, J.M., Lias, J.H., et al. Erosional valleys in the Thaumasia region of Mars: hydrothermal and seismic origins. J. Geophys. Res. 103, 31407–31419, 1998.

Taylor, G.J. Ancient lunar crust: origin, composition, and implications. Elements 5, 17–22, 2009.

Whitford-Stark, J.L. Charting the Southern Seas: the evolution of the lunar Mare Australe.In: Proc. Lunar Planet. Sci. Conf. 10th, 2975–2994, 1979.

Wilhelms, D.E. The geologic history of the Moon, U.S. Geol. Surv. Spec. Pap. 1348, 1987.

Wilhelms, D.E., McCauley, J.F. Geologic map of the near side of the Moon. USGS Map I-0703, scale 1:5000,000, 1971.

Wilhelms, D.E., El-Baz, F. Geologic map of the east side of the Moon. USGS Map I-948, scale 1:5000,000, 1977.

Wilhelms, D. E., Howard, K. A., Wilshire, H. G. Geologic map of the south side of the Moon. USGS Map I-1162, scale 1:5000,000, 1979.

Yamashita, N., Hasebe, N., Reedy, R.C., et al. "Uranium on the Moon: Global distribution and U/Th ratio", Geophys. Res. Lett. 37, L10201, 1–5, 2010.